Available online at www.sciencedirect.com
SCIENCE DIRECT®
ELSEVIER
European Journal of Mechanics B/Fluids 25 (2006) 302–320
EUROPEAN JOURNAL OF MECHANICS B/FLUIDS

An experimental study of the bulk properties of vortex rings translating through a stratified fluid

M.M. Scase *, S.B. Dalziel

Department of Applied Mathematics and Theoretical Physics, University of Cambridge, Centre for Mathematical Sciences, Wilberforce Road, Cambridge, CB3 0WA, UK

Received 31 January 2005; received in revised form 20 July 2005; accepted 5 September 2005

Available online 28 October 2005

Abstract

Experiments are carried out to find the bulk properties and some structural properties of vortex rings in a stratified fluid. Previous theoretical descriptions of vortex ring propagation speed in a homogeneous fluid are compared to experiment and developed for use in stratified fluids. Vortex rings are fired at oblique angles to the horizontal and at different speeds through a stratified fluid. The buoyancy frequency of the fluid is varied between different series of experiments.

New models are proposed which predict the speeds and trajectories of vortex rings fired through a stratified fluid and these are compared to experiment. It is shown that these models perform well in high Froude number flows, but less well in low Froude number flows.

Keywords: Vortex; Ring; Stratified; Buoyancy

1. Introduction

Many turbulent flows are characterised by identifiable structures and in particular by characteristic recurrent forms that are collectively referred to as coherent structures (e.g. Holmes et al. [1]). In many cases such structures contain a significant fraction of the local energy. Coherency entails that these structures tend to persist in time and often provide an effective mechanism for the transfer of energy between different regions of the flow.

This paper concentrates on the behaviour of a particular three-dimensional coherent structure, a vortex ring, in an initially quiescent stratified fluid. In studying the response of the vortex ring to the stratification, and the response of the stratification to the vortex ring, a greater understanding of turbulence in density stratified environments is sought.

It is well known that large sections of the oceans (Bryan and Cox [2] and Gill [3]) and the atmosphere (e.g. §3.1 Lighthill [4], Gill [3]) have stable, continuously stratified densities. These density stratifications restrict vertical motion, gravity acts as a restoring force. Consequently motion tends to be restricted to horizontal planes, and is often referred to as 'layerwise-two-dimensional', or 'quasi-two-dimensional'.

* Corresponding author.
E-mail address: m.scase@damtp.cam.ac.uk (M.M. Scase).

0997-7546/$ – see front matter
doi:10.1016/j.euromechflu.2005.09.003

1.1. Vortex rings as models for coherent structures in turbulent flows

Several key studies have used the vortex ring in a homogeneous environment as a simple example of a coherent structure, regarding it is an idealised turbulent eddy. Maxworthy [5] suggests that the mechanisms by which vortex rings entrain fluid are similar to those by which turbulent fluid entrains laminar fluid at a turbulent-laminar interface. "The observed entrainment process could be of great importance in understanding the mechanism by which turbulent interfaces grow and remain sharp. In fact, by regarding the vortex ring as a model turbulent eddy which, when it reaches the turbulent-laminar interface, is able to entrain fluid by a process involving viscous diffusion, a new attack on one of the more interesting aspects of turbulent motion might be possible" (Maxworthy [5]). Linden [6] successfully used a vortex ring interacting with a density step as a model for plume entrainment and grid generated turbulence. "The assumption that a vortex ring acts as an 'idealised eddy' appears to be quite plausible in Turner's [7] experimental arrangement" [on turbulent entrainment across a density interface] (Linden [6]). It was also suggested (Linden [6]) that for an energy containing eddy to be considered a coherent entity, its velocity of propagation would have to be related to its vorticity structure in a manner similar to that for a spherical vortex.

Fraenkel [8] proved that there exist solutions to the Euler equations in the form of steady vortex rings with small cross-sectional core areas. This work was later generalised in Fraenkel [9] to allow an arbitrary distribution of vorticity on streamlines in the core, although the core size was still assumed to be small compared with the diameter of the ring. Norbury [10] proved the existence of a one-parameter family of vortex rings with constant core vorticity in this inviscid limit. At one end of the parameter range were Fraenkel's small cross-section vortex rings and at the other end was Hill's [11] spherical vortex ring. Norbury was able to calculate the core boundary shape and propagation velocity as well as various other properties.

Each member of Norbury's family of vortex rings propagates with constant velocity. However, it was noted by Reynolds [12] almost a century earlier that vortex rings slow down and their volume increases as they propagate since "...they are continually adding to their bulk water taken up from that which surrounds them and with which their forward momentum must be shared". Motivated by this Maxworthy [5] developed an impulse conserving model based on the empirical result that the vortex ring's velocity of translation decays exponentially with distance from the origin (the Kelvin impulse is conserved between the vortex ring and its wake). This model successfully predicted the propagation speed of the vortex ring, and its volume, without explicitly considering the internal dynamics of the vortex ring. Maxworthy also discussed mechanisms for vortex breakdown. He noticed that the main mechanism for a laminar vortex ring to breakdown was an unstable azimuthal wave propagating around the vortex ring, the amplitude of which grew in time. Eventually the amplitude of this wave is sufficiently large to cause the vortex ring to lose coherency and breakdown. This breakdown mechanism was studied further by Widnall and Sullivan [13] and Widnall and Tsai [14].

1.2. Stratified fluids

One crucial difference between fully three-dimensional flows and two-dimensional flows is the ability in three dimensions for the vorticity to be stretched. This occurs in all three-dimensional turbulent flows and is responsible for the energy cascade being from large scale structures to small scale structures. In three-dimensional turbulence, smaller eddies are subjected to the strain field of the larger eddies resulting in an increase in vorticity (and therefore energy) of the smaller eddies, at the expense of the larger eddies. In two dimensions this is not the case, in fact the energy cascade is in the opposite direction from small scales to large scales. This is as a result of the flow in two dimensions conserving both kinetic energy and enstrophy. Enstrophy can be considered to be a measure of the total vorticity of a flow and is the second moment of the spectral energy distribution. It was shown by Fjørtoft [15] and Charney [16] that if the kinetic energy and enstrophy are to be conserved, any flux of energy towards structures with a large wavenumber must be compensated for by a much larger flux of energy towards structures with small wavenumbers. This has the effect of 'self-organising' turbulence in two dimensions. From a disorderly, arbitrary initial situation – in which the various characteristics are distributed continuously over the whole wavenumber spectrum – one sees the development of so-called vortex structures (Fornberg [17], McWilliams [18], van Heijst [19]).

Experiments where patches of initially fully three-dimensional turbulence were allowed to interact with a background stratification and become quasi-two-dimensional were investigated in Flór [20]. Fluid was forced through a nozzle into a tank, simultaneously viewed from above and through the side of the tank. This showed the vertical scales

in the flow collapsing, and the horizontal scales growing until the flow could be considered quasi-two-dimensional. The initially turbulent flow self-organised itself into a horizontally propagating dipole. This showed that the conditions for self-organisation to occur were not restricted to ideal fluids with precisely two-dimensional flows. In fact satellite imagery well illustrates the abundant presence of large-scale vortices in the oceans and the atmosphere. The motions involved here are quasi-two-dimensional due to the density stratification, the rotation of the system, or a combination of both (van Heijst [19]). Fully three-dimensional flows developing into quasi-two-dimensional flows occur regularly in environmental situations, for example, buoyant plumes produced by industrial chimneys or indeed volcanoes. These plumes rise and entrain ambient surrounding air until they reach their neutral buoyancy level and then spread out in a quasi-two-dimensional fashion in this plane. Understanding this transition from three-dimensional flow to quasi-two-dimensional flow is therefore key to understanding many turbulent environmental flows.

Orlandi et al. [21] considered a vortex ring propagating vertically contrary to the buoyancy force it experienced, and developed an argument for the penetration depth based on the baroclinic generation of vorticity of the opposite sign to that found in the core of the ring. For the present study momentum and the buoyancy force have been used directly, rather than taking their curl and working with vorticity and baroclinic generation. While there is a formal similarity between these approaches, there is a question as to whether asymmetry in the spatial distribution of baroclinic generation – or equivalently in inhomogeneity in the buoyancy force – may play a role in altering the course of the vortex ring.

Consider the case where the ring has a core of uniform density that is less than that of its surroundings and is propagating at an angle to the vertical. The density differences are (on average) greater on the lower side of the ring, so baroclinic generation on the lower side of the ring would be greater than that on the upper side of the ring. The stronger baroclinically-generated vorticity on the lower side will tend to advect the lower side upwards relative to the upper side, steering the axis of the ring towards the vertical regardless of whether the ring is propagating upwards or downwards. While it might be argued that there will be some asymmetry in the vorticity subsequently entrained into the vortex ring (which may then affect its path), it is noted that the assumed homogeneity of density within the ring that created the asymmetry in baroclinic generation can only be justified if the vorticity within the ring is also homogeneous. Similar arguments apply when the ring is denser than it surroundings, with the steering again acting towards the vertical.

Careful consideration of the above arguments shows that asymmetric baroclinic generation will only steer the ring when the ring is not spherical. Moreover, the same steering may be seen from buoyancy arguments by considering the couple experienced by a non-spherical vortex ring of uniform density, and that the steering mechanism vanishes for rings propagating at their own neutral buoyancy level. For the present study it is believed that this steering mechanism has a negligible effect compared with the direct buoyancy force included the model. It is noted, however, that this baroclinic steering may help to stabilise rings propagating vertically through a stratification, such as those considered by Orlandi et al. [21].

In terms of the theoretical models presented in this paper, it will be assumed throughout that the fluid is unbounded. When the fluid is considered to be stratified it will be assumed to have a uniform density stratification $\rho_0(z) = \rho_{00}\exp\{-\lambda z\}$, where $\lambda g = N^2$. Here, N is the constant buoyancy frequency defined by

$$N^2 = -\frac{g}{\rho_0}\frac{\mathrm{d}\rho_0}{\mathrm{d}z}, \tag{1}$$

with g the acceleration due to gravity, ρ_{00} a reference density and $\rho_0(z)$ the background, hydrostatic density field. Where the Boussinesq approximation (Boussinesq [22]) is made, the factor g/ρ_0 is replaced by g/ρ_{00} in (1) since $\rho_0 \simeq \rho_{00}(1-\lambda z)$.

The relevant nondimensional parameters characterising the flows considered are the Reynolds and Froude numbers defined respectively as

$$Re = \frac{2Ua}{\nu}, \qquad Fr = \frac{U}{Na}, \tag{2}$$

where U is a characteristic velocity and a is half the vertical core-to-core distance of the vortex ring.

2. Experimental set-up

The basic experimental set-up is shown in Fig. 1. The experimental tank had dimensions 2.5 m × 0.7 m × 0.8 m and was raised on legs so that a mirror could be positioned underneath. Behind the tank was a 2.0 m × 1.0 m light bank using 6 pairs of 70 W high frequency fluorescent tubes. A Camelia 8 Megapixel digital camera was used to capture the experiments. The camera's resolution was 3500 × 2300 pixels with a frame rate of approximately 2.1 frames per second. This camera was used in conjunction with a liquid crystal shutter and a Nikon Zoom lens (Nikkor 35 ∼ 135 mm F 3.5 ∼ 4.5). This meant the experimental frames captured were high in spatial resolution but relatively low in temporal resolution compared to the initial turnover time of the vortex ring. The experimental set-ups in both Section 2.1 and Section 2.2 are identical, except that the ambient fluid is stratified in Section 2.2.

The vortex ring was created by using a hand pump to force a slug of fluid out of an L-shaped tube, with a 4.4×10^{-2} m bore (see Fig. 1), positioned in the fluid. As the fluid was forced out of the tube an unsteady boundary layer formed adjacent to the inner wall which quickly separated at the tube outlet. The ejected cylindrical vortex sheet then rolled up into the vortex ring. This method of creating vortex rings was not very repeatable, due to the manual actuation of the pump, but was necessary as a large range of Froude and Reynolds number vortex rings were required. The vortex ring was marked by placing neutrally buoyant dye (red food colouring) in the opening of the tube. The dye was assumed to be a passive scalar when advected by the flow, but which does not affect the flow. The diffusivity of dye and salt is approximately three orders of magnitude less than the diffusivity of the vorticity. This means that whilst the dye does not mark the full extent of the vortex ring, it does mark the core positions. To stop a build up of dye in the tank, bleach was added after several runs had been completed. This was done carefully using a syringe and caused a negligible amount of mixing compared to an individual experimental run.

After the tank was filled a large wire mesh, of known mesh-size, was placed in the tank. From this a mapping from the pixel coordinates, captured by the camera, to 'real world coordinates' was generated, allowing the size and position of the vortex ring to be established. At each time step (camera frame rate) the positions of the two visible vortex core centres (see Fig. 2) were noted using the world coordinate system. Figs. 2, 4–7, 9 and 10(b) use an arbitrary false colour scheme.

Ideally the centre of the vortex cores are stagnation points of the flow in the frame of reference of the vortex ring centre. From the positions of the vortex cores, the position of the vortex ring and the vertical core-to-core distance were recorded. In some instances, for example as the vortex ring collapses, the position of the cores is not well-defined and so an estimate of their approximate position is recorded.

For the stratified experiments of Section 2.2 it was of interest to see how the stratification restricted vertical fluid motions and caused a quasi-two-dimensionalisation of the flow. In order to visualise this, the camera was positioned so that the vertical profile (side view) of the vortex ring could be seen directly, and the horizontal profile (plan view) could be seen through the mirror.

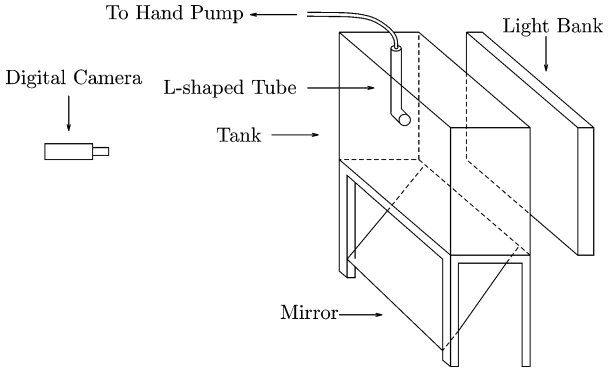

Fig. 1. Experimental set-up for vortex ring experiments. Dyed vortex rings are forced out of the L-shaped tube. The tank is lit from behind by a light bank and the experiments are recorded using a digital camera.

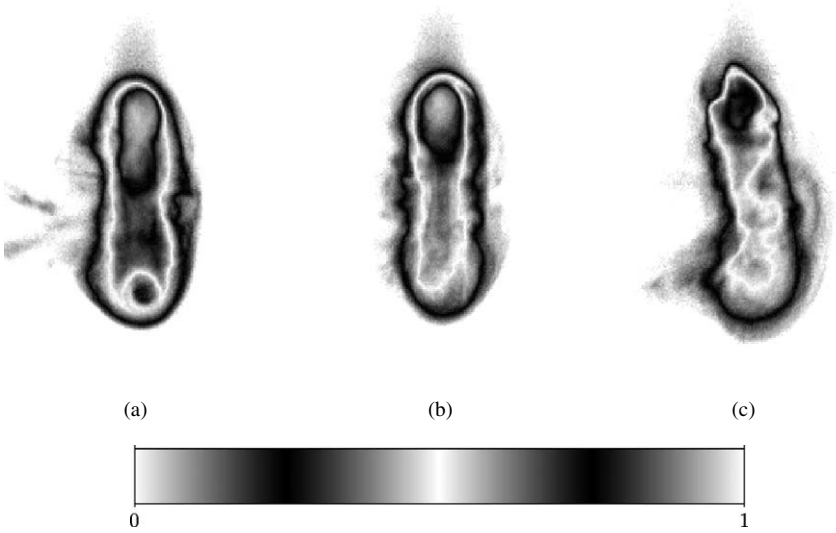

Fig. 2. Vortex core positions for a vortex ring at three different times; (a) $t = 5.9$ s, $Re = 3800$, (b) $t = 11.9$ s, $Re = 2800$, (c) $t = 17.8$ s, $Re = 2100$. The vortex cores are stagnation points for the flow in the frame of reference of the vortex ring. The false colour used in this figure and Figs. 4–7, 9, 10 is used only as a marker for the position of the vortex ring.

2.1. Experiments in homogeneous fluid

The fluid used in these experiments was mains supply water. It was left to settle over a period of two days to allow the fluid to reach thermal equilibrium. This meant the air dissolved in the water came out of solution and the resulting bubbles were removed. Gravity does not play a role for experiments conducted in a homogeneous ambient background fluid since no buoyancy forces are acting. Hence the position of the vortex ring is denoted, without loss of generality, as $\boldsymbol{x}(t) = (x(t), 0, 0)$, where the x-axis is aligned with the direction of propagation.

The theory of Maxworthy [5] states that the initial impulse given to the vortex ring is conserved throughout the motion (i.e. the motion of the vortex ring and that of the wake). The vortex ring is sometimes referred to as a 'bubble' in the text (e.g. Maxworthy [5]). It was found empirically that the vortex ring's speed, $\dot{x}$, decayed exponentially with distance, x, from the origin. The model proposed by Maxworthy suggests that the vortex ring starts at $x = -\infty$ and time t_∞ where $-\infty < t_\infty \leqslant 0$ such that $\dot{x}(t) \sim (t - t_\infty)^{-1}$, $\dot{x}(0) = \dot{x}_0$ and $x(0) = 0$. This also implies that at $t = t_\infty$ the vortex ring has infinite velocity. The assertion that $\dot{x}$ decays exponentially with distance, x, from the origin is tested here to confirm both that the experimental set-up works and that Maxworthy's theory is suitable for extending for the stratified case.

If the velocity decreases exponentially with distance from the origin then

$$\log\left(\frac{\dot{x}}{\dot{x}_0}\right) = -\mu x, \tag{3}$$

where μ is a positive constant with dimensions of inverse length. This implies that the temporal origin, t_∞, is given by $t_\infty = -1/\mu\dot{x}_0$, the position of the vortex ring is given by

$$x(t) = \frac{\log(\mu\dot{x}_0 t + 1)}{\mu} = \frac{\log(\mu\dot{x}_0[t - t_\infty])}{\mu}, \tag{4}$$

and the propagation velocity is given by

$$\dot{x}(t) = \frac{\dot{x}_0}{\mu\dot{x}_0 t + 1} = \frac{1}{\mu(t - t_\infty)}. \tag{5}$$

This satisfies Maxworthy's requirement that $\dot{x}(t) \sim (t - t_\infty)^{-1}$.

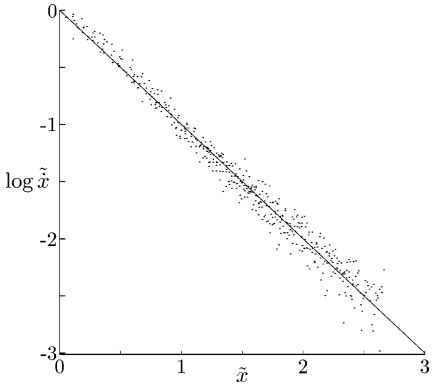

Fig. 3. The logarithm of the propagation velocity of the vortex ring against position, nondimensionalised to lie on $\log \tilde{\dot{x}} = -\tilde{x}$. A total of 485 data points are used. Initial Reynolds numbers ranged from 1500 to 10 500.

Twenty vortex rings were fired and their positions were measured at time steps of $t = 0.47$ s. Their velocity was calculated by centrally differencing about their current position, i.e. if their position and time at the mth time step is given by (x_m, t_m) then

$$\dot{x}(t_m) \approx \frac{x_{m+1} - x_{m-1}}{t_{m+1} - t_{m-1}}. \tag{6}$$

The constant μ and initial velocity $\dot{x}_0$ were found by least-squares regression on $\log \dot{x}$ against x (see Eq. (3)).

It might be anticipated that knowledge of the initial velocity of the vortex ring would be sufficient to predict the subsequent motion. However, the above analysis shows that this is not the case. The problem lies in the fact that since $x(t_\infty) = -\infty$ there is not sufficient information to calculate μ (this would not be the case if $x(t_\infty) > -\infty$). This is because a vortex ring at $x = 0$ at $t = 0$ could have arrived there in an infinite number of ways, i.e. there are an infinite number of possible vortex ring histories to get to $x = 0$ at $t = 0$ from $x = -\infty$ at $t = t_\infty$. The vortex ring is at a different point of its exponential decay for each of the histories, and will therefore continue to decay at different rates depending on the history. This means that knowledge of the position, or size, of the vortex ring at some other time must be gained before the subsequent motion can be accurately predicted. This essentially means that μ cannot be calculated from knowledge of either the initial velocity or initial Reynolds number alone.

The origin correction is a mathematical way of modelling the vortex ring generation process. The internal distribution of vorticity in the vortex ring depends on way the vortex ring is generated. This distribution of vorticity governs how the vortex ring will propagate. Maxworthy's model means that the effects of the distribution of vorticity can be modelled with two parameters. Even though all the vortex rings used in the experiments were generated using the same basic method there were many variables which could affect the type of vortex ring. Examples include the stroke length of the pump (and hence the ratio of slug length to ring diameter) and the velocity profile of the pumping action.

Fig. 3 shows the data from the experiments collapsed onto the line $\log \tilde{\dot{x}} = -\tilde{x}$, for illustration, where $\tilde{\dot{x}} = \dot{x}/\dot{x}_0$ and $\tilde{x} = \mu x$ are nondimensional. A total of 485 data points are used and the range of initial Reynolds numbers was from 1500 to 10 500. The graph shows a good fit, the slight flaring towards the right hand end of the graph (approaching $\tilde{x} = 3$) is due to the difficulty in measuring the small movements of the vortex ring precisely, and hence the errors in the velocity are larger. The goodness of fit indicates that Maxworthy's model is a good model for vortex rings propagating in a homogeneous fluid, and that the experimental set-up devised for the current investigation works.

Fig. 4 shows a comparison between the structures of a vortex ring in the (x, z) and (x, y) planes. As is expected, since no buoyancy forces are acting, the ring looks qualitatively the same in both aspects.

The volume of the vortex ring increases as it propagates through the fluid. This increase in volume occurs because the vortex ring entrains ambient fluid as it propagates. Maxworthy [5] suggests that the rate of increase of volume is constant and that the volume, V, obeys

$$\frac{1}{V}\frac{\mathrm{d}V}{\mathrm{d}t} = \frac{1}{t - t_\infty} = \mu \dot{x}. \tag{7}$$

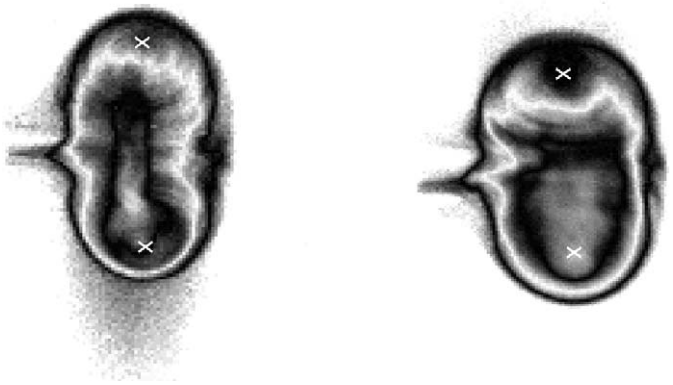

(a) (b)

Fig. 4. (a) is the (x, y) profile of a typical vortex ring in the homogeneous fluid; (b) is the (x, z) profile of the same ring at the same time. The structure of the ring is approximately the same in both aspects. The approximate positions of the vortex cores are marked with crosses.

With the initial condition $V(0) = V_0$ this gives the result

$$V(t) = V_0 e^{\mu x} = V_0 \left(\frac{t - t_\infty}{|t_\infty|} \right), \tag{8}$$

which implies that at $t = t_\infty$, $V = 0$.

As first investigated in Widnall and Sullivan [13] and further discussed in Widnall and Tsai [14] the main method of vortex ring collapse in a homogeneous fluid is caused by azimuthal wave propagation around the vortex ring core. This was demonstrated experimentally by Widnall and Sullivan [13], and Didden [23] and also shown in Van Dyke [24]. As the ring propagates forwards, the amplitude of the wave increases until it eventually pinches-off and the ring collapses. However, as will be seen in Section 2.2 there is a different method of breakdown for a vortex ring propagating through a stratified fluid.

2.2. Experiments in stratified fluid

The stratification was created using the well-known 'double-buckets' technique (Fortuin [25]). This technique creates nominally linear density stratifications. Samples of fluid were taken from the tank and the density measured with a digital refractometer. Least squares linear regression was used for both a linear fit and an exponential fit to estimate the buoyancy frequency. The difference in the calculated values for N and ρ_{00} between the linear fit and the exponential fit was typically of the order of 0.02%.

When a neutrally buoyant vortex ring propagates horizontally through a density stratification the fluid it entrains is, on average, of the same density as that already contained within the ring. Therefore, there are no net buoyancy forces acting on the ring which will cause it to deflect from its initial propagation direction. This is not true for any other angle of propagation. For this reason, a series of experiments were run with a vortex ring propagating horizontally through a density stratification. Since there is no net change in the density of the vortex ring, this ensures that the effects of the entrainment into the vortex ring of fluid of varying density are minimised. The velocity profiles of these vortex ring experiments are compared to the expected profile predicted by Maxworthy [5] for a vortex ring propagating through a homogeneous fluid.

2.2.1. Horizontally propagating vortex rings

The vortex ring's position was measured as in Section 2.1 and recorded. Since the vortex ring is only propagating in a horizontal direction and does not deviate from this trajectory, its position is given as in Section 2.1 by $\boldsymbol{x}(t) = (x(t), 0, 0)$.

The wake behind the vortex ring, due to vorticity shed by the vortex ring, mixes the density stratification irreversibly as can be observed by eye after a series of experiments have been performed. It is assumed that once the wake is formed

behind the vortex ring it is no longer maintained by the vortex ring itself. Therefore the wake kinetic energy that is lost to viscous dissipation, and to the potential energy gained by the background fluid through irreversible mixing has already been given by the vortex ring to the wake. Accordingly the mixing of the stratification by the wake of the vortex ring is not an extra energy sink on the vortex ring. Hence the modelling in Section 3 will neglect the effect of the stratification on the wake.

Figs. 5–7 are dye images showing the development of the structure for a typical vortex ring propagating horizontally through a density stratification. Fig. 5 shows the development of the vortex ring shortly after it is generated. The vortex ring is moving quickly (i.e. with high Froude number), and the effects of the stratification can be considered negligible. The structure of the vortex ring looks qualitatively similar in the (x, y) and (x, z) planes. The dye has density $\rho_{00} \sim 1.04 \times 10^3$ kg m^{-3} and is neutrally buoyant at $z = 0$. As it is detrained behind the vortex ring it quickly returns to its neutrally buoyant level and this is why the wake appears thin in Figs. 5(a)–(c) (of order 1×10^{-2} m) but appears relatively wide in Figs. 5(d)–(f) (of order 5×10^{-2} m). The ring has the same length scale in both aspects and remains thick-cored. As was discussed in Section 1, the stratification restricts vertical motions of the fluid, leading to a quasi-two-dimensionalisation of the flow. This can be seen from a qualitative comparison of the structure of the vortex ring in the (x, y) and (x, z) planes (Figs. 5–7), analogously to Fig. 4.

At late times, Fig. 6 shows the collapse of the vortex ring (the same ring as that in Figs. 5 and 7) from a fully three-dimensional structure to a quasi-two-dimensional structure. In Figs. (a) and (d), the 'vortex ring' is less clearly defined than in Fig. 5, it has a finer structure around the surface of the ring, with smaller length scales clearly visible, and the wake has a much finer structure too. The vortex ring is said to be in the early stages of a transition to turbulence, whereby structures on many scales appear within the vortex ring which were not there before. In Figs. (b) and (e) the structure can no longer be considered a coherent vortex ring. The structure is clearly not self-similar as it has become smaller in the (x, z) plane but has expanded in the (x, y) plane. By Figs. (c) and (f) the lack of vortex stretching due to the stratification, and the resulting inverse energy cascade, has led to the structure reforming coherently as a dipole. There are still some observable small scale structures, but fewer than in (b) and (e).

Fig. 7 shows the dipole and the wake left by the propagating vortex ring after a long time ($t > 1000$ s). The horizontal extent of the structures are order 10 times greater than the vertical extent. The original vortex ring is now a very flat and coherent dipole. The wake which contained many small scale structures in Fig. 6 now contains mainly large scale structures.

The initial effect of the stratification on a vortex ring, with sufficiently high Froude number, is small. This means that the constant μ (see Eq. (3)) can be calculated approximately from the first few data points. From this the expected trajectory, under Maxworthy's model for vortex rings propagating in a homogeneous fluid, can be calculated and compared to what was observed for the vortex ring propagating in a stratified fluid. This comparison is shown in Fig. 8. The solid line is the expected position of the vortex ring if it were propagating in a homogeneous fluid, the points are data points recorded from experiments with a range of initial Froude numbers. The constant μ is calculated from the first 7 data points for each experiment (between $t = 0$ s and $t = 2.8$ s) and is reasonably insensitive if the number of data points chosen is between 5 and 10 (the variation is of order 10%). The axes have been nondimensionalised with $\tilde{x} = \mu x$, as in Fig. 3, and $\tilde{t} = \mu \dot{x}_0 t$. The data points are from 8 different vortex rings with initial Froude numbers varying from $Fr = 2.9$ to $Fr = 14.8$ and initial Reynolds numbers varying from approximately $Re = 1200$ to $Re = 6200$. In each case the distance travelled by the vortex ring in a given time is less than would be expected if it were propagating in a homogeneous fluid.

2.2.2. *Vortex rings propagating at an oblique angle*

Vortex rings are fired at oblique angles to simulate the behaviour of coherent structures in turbulent flows. The position of the vortex ring is now given by $\boldsymbol{x}(t) = (x(t), 0, z(t))$.

A neutrally buoyant vortex ring is formed, in this experimental set-up, but as it propagates away from $z = 0$ this is no longer the case. If it propagates in the direction of increasing z the vortex ring is denser than the surrounding ambient fluid, if it propagates in the direction of decreasing z the vortex ring is less dense than the surrounding fluid. In both cases the vortex ring will experience restoring buoyancy forces as a result of the difference in densities, and the effects of gravity cannot be ignored. The effect of these buoyancy forces is to make the vertical position of the vortex ring oscillate since it experiences a buoyancy force downwards as it rises and a buoyancy force upwards as it sinks.

Fig. 9 shows the (x, z) profile of a vortex ring fired at 105° to the upright vertical with initial Froude number $Fr = 6.7$ and Reynolds number $Re = 6000$. The images show that although the vortex ring initially propagates downwards

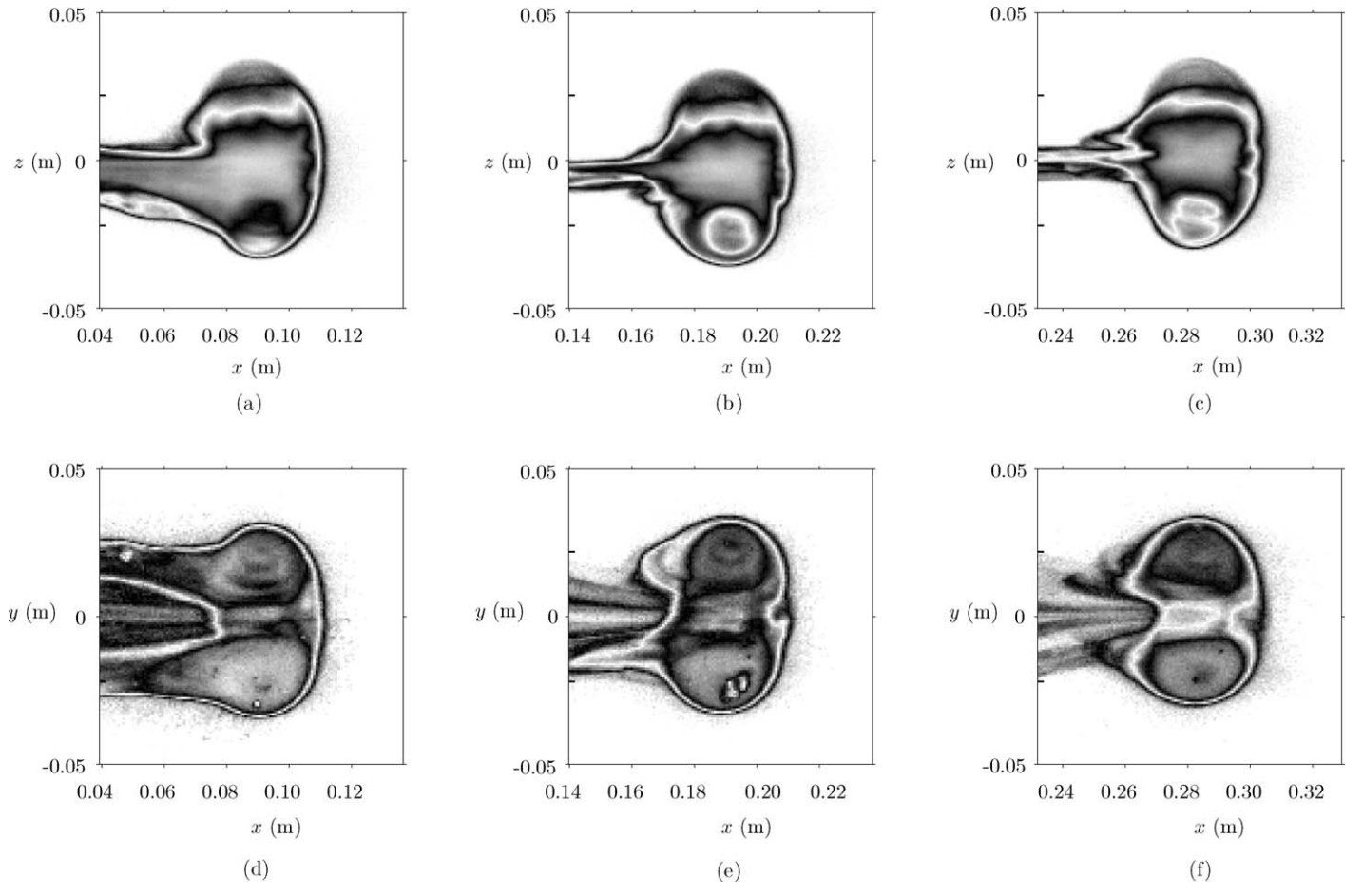

Fig. 5. (a)–(c) are the (x, z) profiles of a vortex ring in a stratified fluid, separated by a time interval of approximately 2 s. (d)–(f) are the corresponding (x, y) profiles. The thick black tick marks on the vertical axes indicate the diameter of the tube opening. The initial speed of the vortex ring was $\dot{x}_0 = 5.4 \times 10^{-2}$ m s^{-1}. (a) and (d) are at $t = 3.7$ s; (b) and (e) are at $t = 6.1$ s; (c) and (f) are at $t = 8.4$ s. The buoyancy frequency was $N = 0.93$ s^{-1} and the initial Froude number was $Fr \sim 2.6$. Initially the stratification has little effect on the vortex ring.

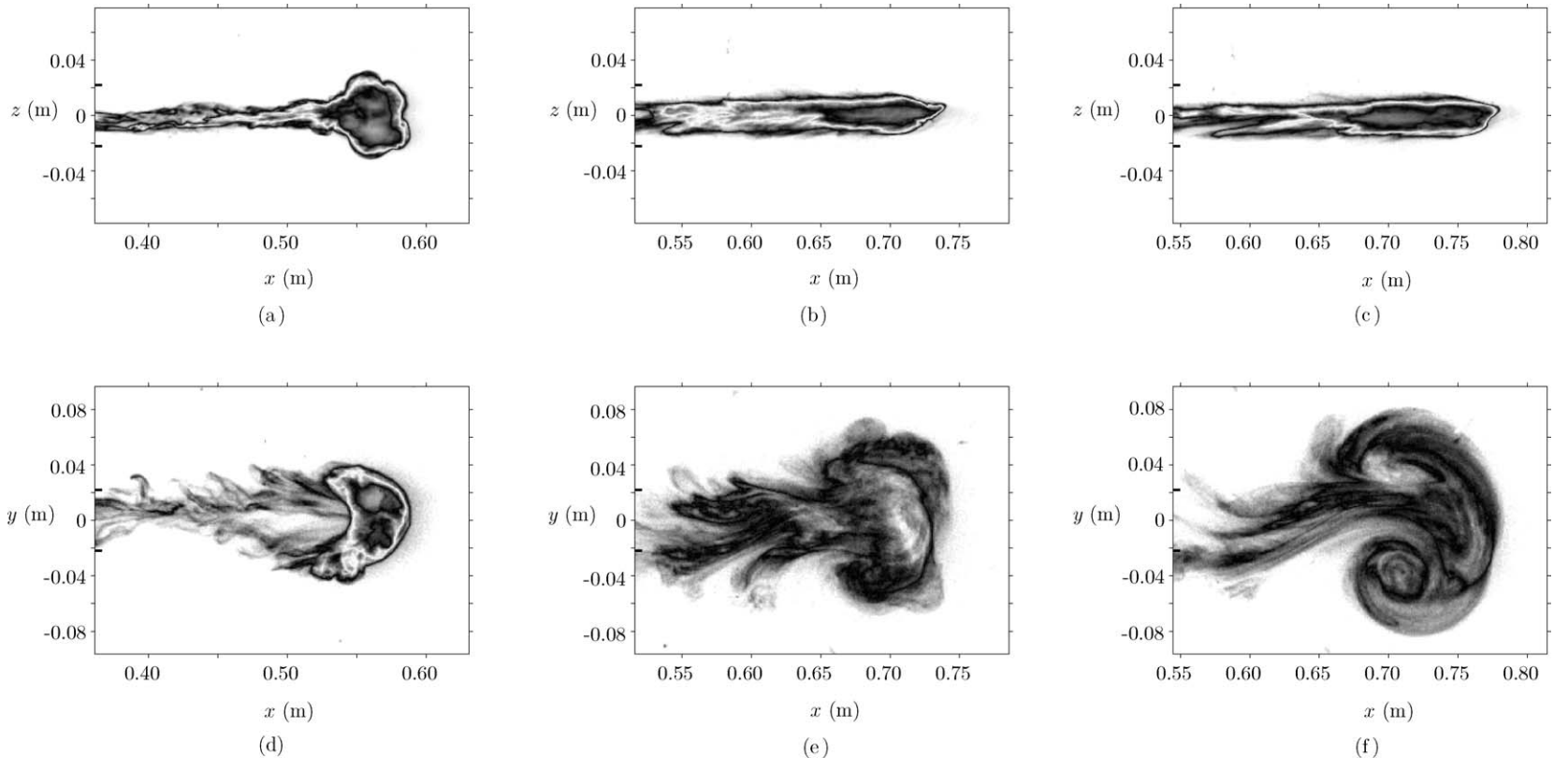

Fig. 6. (a)–(c) are the (x, z) profiles of a collapsing vortex ring in a stratified fluid, separated by a time interval of approximately 20 s. (d)–(f) are the corresponding (x, y) profiles. The thick black tick marks on the vertical axes indicate the diameter of the tube opening. These images are from the same experiment as in Fig. 5 but (a) and (d) are at $t = 17.8$ s; (b) and (e) are at $t = 41.1$ s; (c) and (f) are at $t = 64.5$ s. The initial Froude number was $Fr \sim 2.6$. The stratification restricts the vertical motion causing a quasi-two-dimensionalisation of the flow.

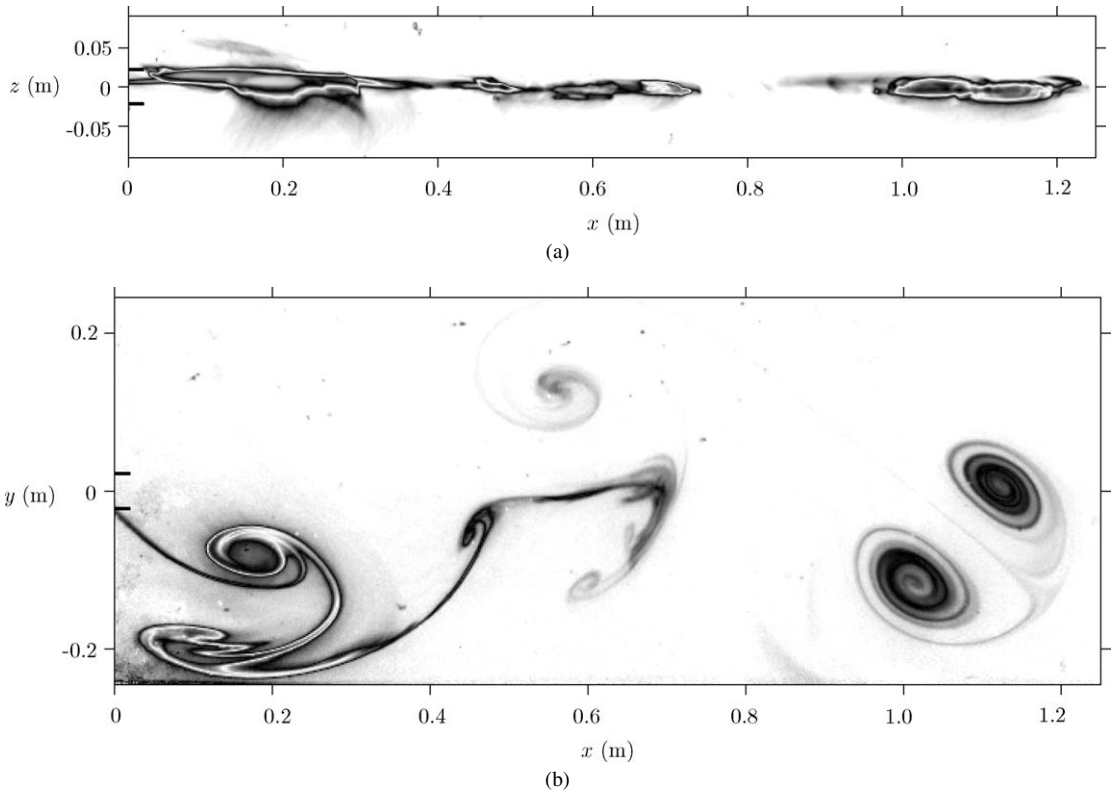

Fig. 7. (a) Shows the profile of the same vortex ring as in Figs. 5 and 6 collapsing into a thin layer in the (x, z) plane; (b) shows how after a long time ($t \approx 1380$ s), coherent structures are formed in the (x, y) plane. The initial Froude number was $Fr \sim 2.6$. The thick black tick marks on the vertical axes indicate the diameter of the tube opening.

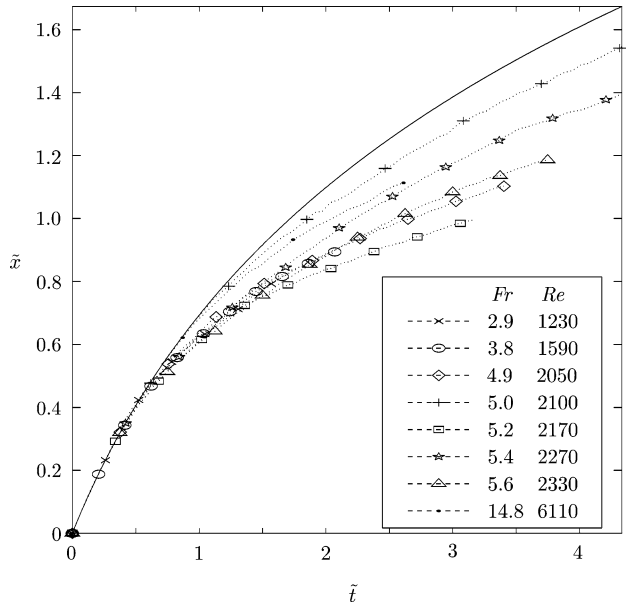

Fig. 8. Positions of horizontally propagating vortex rings through stratified fluid up to some nominal time of collapse beyond which they cannot be followed as coherent entities. The solid line shows the expected position of the vortex ring if it were propagating in a homogeneous fluid. The dashed lines are the location of the vortex ring in the experiments. The constant μ is calculated from the first 7 data points. The axes have been nondimensionalised with $\tilde{x} = \mu x$ and $\tilde{t} = \mu \dot{x}_0 t$. The cases with lower initial Froude number tend to collapse earlier.

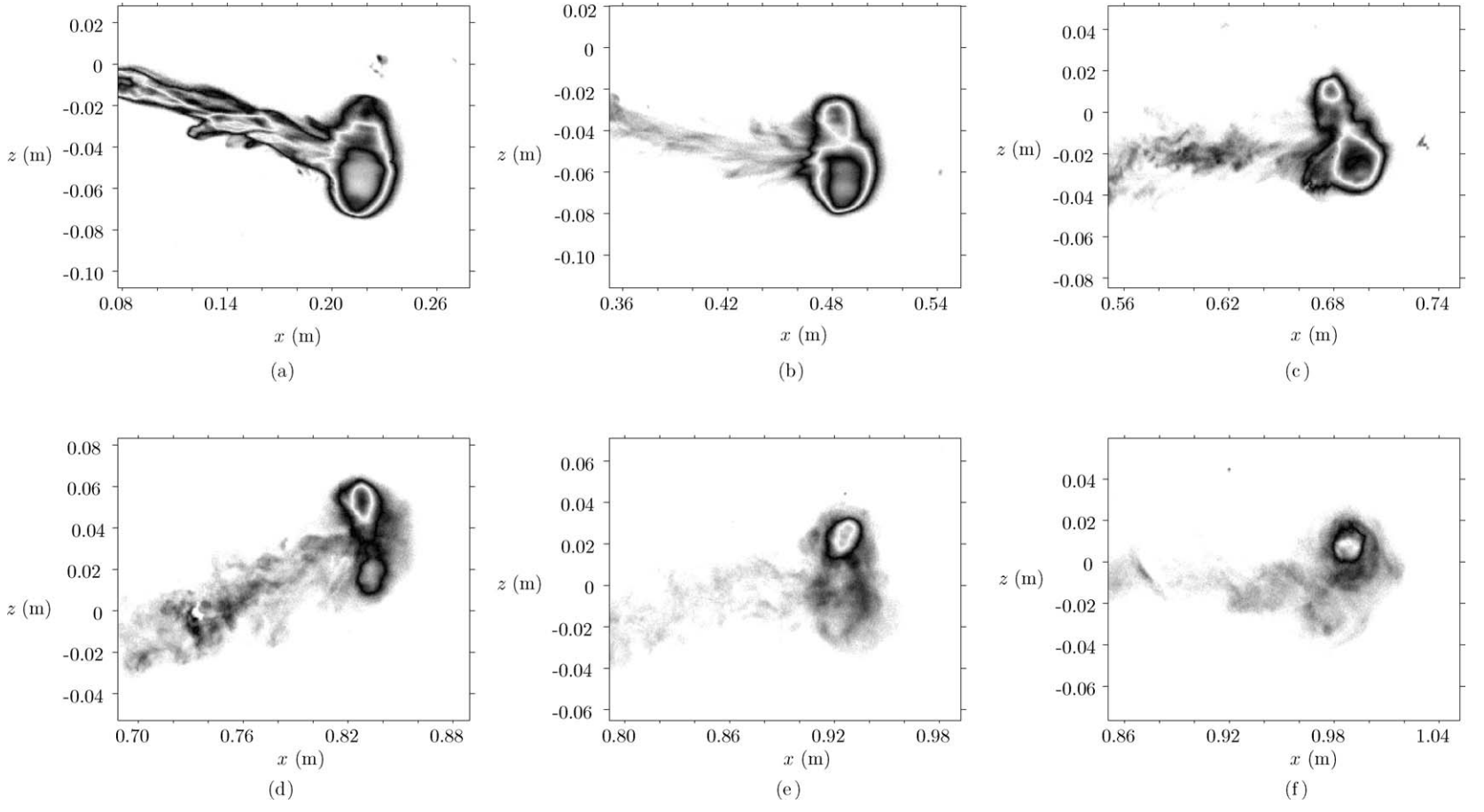

Fig. 9. A vortex ring fired at 105° to the upward vertical with initial radius 4.4×10^{-2} m and initial velocity 1.4×10^{-1} m s^{-1} into a stratification with $N = 0.93$ s^{-1}. The images are separated by $t = 2.3$ s with (a) at $t = 0.94$ s.

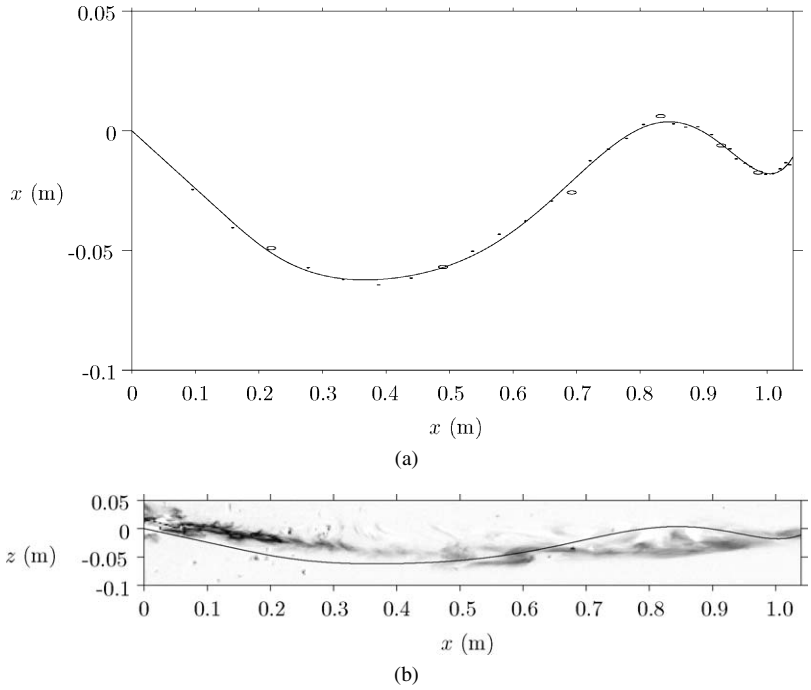

Fig. 10. Track of a vortex ring with initial radius 4.4×10^{-2} m fired at 105° to the vertical with initial velocity 1.4×10^{-1} m s^{-1} in a stratification with $N = 0.93$ s^{-1}. (a) The points are data points, the circles correspond to Fig. 9(a)–(f) and the solid line is a best fit seventh order polynomial for illustration. (b) Shows the actual track compared with the level at which the dye has detrained and settled out.

into ambient fluid of increasing density (Fig. 9(a)), the buoyancy forces cause the vortex ring to level off (Fig. 9(b)). The vortex ring starts propagating upwards (Figs. 9(c)–(d)) and passes its neutral buoyancy level. The vortex ring is therefore heavier than the surrounding ambient fluid, causing the vortex ring to level off again (Figs. 9(e)–(f)). The sequence of images show that the vortex ring's axis of symmetry tends to be aligned with the direction of propagation, which changes during the motion. This means that the vortex ring pitches forwards and backwards in the $y = 0$ plane as it oscillates. The images also show an increase in the fine structures on the surface of the vortex ring and in the wake as the vortex ring undergoes its transition to a turbulent state. The change in dye concentration shows that the vortex ring has been entraining undyed fluid and detraining dyed fluid throughout its motion. Note that the dye concentration within the ring does not appear to change symmetrically. When the vortex ring is below the neutral buoyancy level the top thins out, and when the vortex ring is above the neutral buoyancy level the bottom thins out.

The track of the vortex ring is shown in Fig. 10(a). It is clear that the vortex ring does not oscillate about its initial neutral buoyancy level $z = 0$. Fig. 10(b) shows the experimental image at $t = 160$ s with the wake clearly visible. This approximates the track of the vortex ring, but is not identical. The dye detrained into the wake is not necessarily neutrally buoyant with respect to the ambient fluid at the time it is detrained and as a result settles out to a different level as the vortex ring propagates away.

As a vortex ring propagates its volume increases, as was discussed in Section 2.1. The fluid it entrains as it increases its volume has density close to $\rho_0(z)$ (i.e. the density of the unperturbed hydrostatic background density at the height of the vortex ring, z). Therefore it is no longer entraining fluid of equal density to the vortex ring and so the height at which the vortex ring can be considered neutrally buoyant changes as it propagates. As a result of this, the height at which the collapsed vortex ring finally settles out depends crucially on the initial conditions of the flow, unlike the horizontal case.

As in the horizontal case discussed in Section 2.2.1, the stratification has a negligible effect on the initial motion of the vortex ring. The vortex ring initially propagates along a straight trajectory. The effect of the stratification, as evidenced by the curvature of the trajectories, is felt only subsequently as the vortex ring moves into fluid of a different density. This means that a constant μ can be calculated for the vortex rings fired at oblique angles as for vortex rings fired horizontally. This will be used in Section 3 to model the motion of the vortex ring.

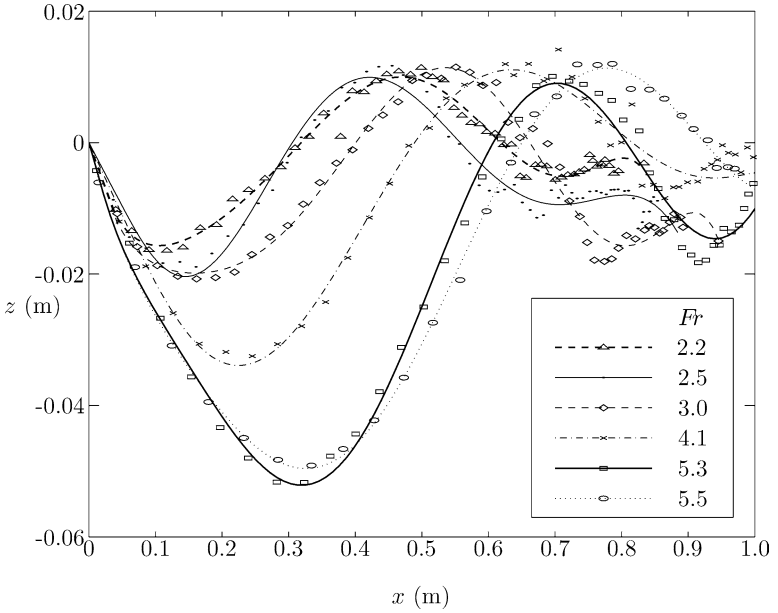

Fig. 11. Six vortex ring tracks from a series of thirty experiments. The initial Froude numbers are shown in the legend. The vortex rings were all fired at an angle of 105° to the upright vertical.

Fig. 11 demonstrates similar behaviour for a range of initial Froude numbers. Shown are six vortex ring tracks, for illustration, from a series of thirty experiments, with six different Froude numbers but all fired at 105° to the vertical (the markers are the data points and the curves are fitted to aid the eye). The figure shows that the vortex rings which have higher Froude numbers penetrate further from their initial neutral buoyancy level. This is expected since a high Froude number may be interpreted as either a weak stratification or high initial speed. The higher Froude number vortex rings also break down later in time than the low Froude number vortex rings in the range of Froude numbers shown. None of the tracks oscillate about $z = 0$ and they all have comparable maximum heights of order $z = 1.2 \times 10^{-2}$ m. This height will clearly depend on the initial conditions although its scaling has not been determined.

3. Entrainment analysis

In Section 3.1, Turner's [26] buoyant vortex ring model will also be discussed, including the main differences between his study and the present one. A variety of models are proposed to predict the bulk positional properties of a vortex ring propagating at an oblique angle through a density stratified fluid in Section 3.2. Finally, in Section 3.3, the models are compared to the experimental data of Section 2.

3.1. Buoyant vortex rings

Turner, [26–28], considered a vortex ring of differing density to its surroundings but uniform within the vortex ring (due to turbulent mixing), with radius R and cross-sectional core radius $a \ll R$ propagating through an ideal fluid. The case when the ring rises through a stably stratified fluid was also considered.

It is assumed that the vorticity of the vortex ring is confined within a region that never extends to the centre of the ring or to the periphery of the vortex ring. It is also assumed that the circulation, Γ, is constant, as if Kelvin's Circulation Theorem applied within the vortex ring. The speed, $|\dot{\boldsymbol{x}}|$, of the vortex ring is proportional to the ratio of the circulation to the ring radius, Γ/R. Unlike the experiments of Section 2, Turner does not use initially neutrally buoyant vortex rings. This means that unlike the present study, the impulse, I, of the vortex ring was not constant. Turner uses the equation for the impulse of the vortex ring, developed by Lamb [29], so that

$$I = \pi \rho_{00} \Gamma R^2. \tag{9}$$

Where ρ is the density of the core of the vortex ring, ρ_0 is the density of the ambient fluid at the height of the vortex ring, and ρ_{00} is the density of the ambient fluid at $z = 0$. It is assumed that the density differences are small compared with ρ_{00} and that ρ is a constant, i.e. there is no entrainment allowed. The rate of change of the impulse is given by the buoyancy force B, defined as

$$B = gV(\rho_0 - \rho), \tag{10}$$

where V is the volume of the vortex ring core, giving $\mathrm{d}I/\mathrm{d}t = B$. In a homogeneous fluid ($\rho_0 \equiv \rho_{00}$), B is constant. The time derivative of (9), using (10), shows that the radius of the ring, R, grows according to

$$\frac{\mathrm{d}R^2}{\mathrm{d}t} = \frac{B}{\pi\rho_{00}\Gamma}, \tag{11}$$

which is constant, meaning that the radius of the vortex ring expands.

In the stratified case ($\rho_0 \neq \rho_{00}$), (11) still holds although B is no longer a constant. It was shown by Turner that a buoyant vortex ring rising through a stratified fluid undergoes a greater increase in radius than a non-buoyant vortex ring. It was also shown that as the buoyant vortex ring rapidly increases its radius, it entrains a significant amount of heavier fluid, unlike the non-buoyant vortex ring. This leads to the perhaps surprising conclusion that very buoyant vortex rings rise to a lower level than a non-buoyant vortex ring in the same stratification.

3.2. Modification of theory to include buoyancy entrainment

A new approach is suggested based on the ideas of both Maxworthy [5] and Turner [26,28], whereby buoyancy entrainment is taken into account. When Maxworthy's empirical relation that the speed of the vortex ring's propagation, $\dot{x}_0$, decays exponentially with distance from the virtual origin (3), is written as the differential equation

$$\ddot{x} + \mu\dot{x}^2 = 0, \tag{12}$$

it shows that the constant μ in (3) can be interpreted as a velocity-squared drag coefficient. Here the drag is not only a form (pressure) drag (§ 5.11 Batchelor [30]) but also accounts for the increase in size due to entrainment.

A simple extension to this model would be to include a buoyancy force but assume that entrainment does not alter the density, ρ_{00}, of the vortex ring. Such a simplistic model would only be suitable for short times or for vortex rings propagating close to the horizontal where the density difference of the entrained fluid to the fluid contained by the vortex ring is negligible. A better model is to allow the vortex ring to entrain fluid with the same density as that of the surrounding fluid, i.e. of density $\rho_0(z)$.

The average density of the stratified background fluid between the heights z and $z + \delta z$, where δz is an arbitrary small distance, is given by

$$\bar{\rho_0} \sim \rho_0(z)\left(1 - \frac{N^2\delta z}{2g}\right) + \mathcal{O}(\delta z^2), \tag{13}$$

for both an exponential and a linear background stratification. In time δt the entrained fluid into the vortex ring will have volume δV and density $\bar{\rho_0}$ giving

$$\rho(t + \delta t) = \frac{\rho(t)V + \bar{\rho_0}\delta V}{V + \delta V}. \tag{14}$$

It is assumed in (14) that the fluid within the vortex ring is homogeneous at each time t, which is not strictly the case. The internal mixing of the fluid within the vortex ring is a viscous process and cannot happen instantaneously. From (13) and (14) it follows that

$$\rho(t + \delta t) \sim \rho(t) + \big(\rho_0(z) - \rho(t)\big)\frac{\delta V}{V} + \mathcal{O}(\delta^2). \tag{15}$$

One further assumption is required and that is that the vortex ring's volume increases by entrainment at the same rate as if the fluid were homogeneous. This assumption will be approximately valid for large Froude number flows, but will not necessarily be true for smaller Froude numbers. Under this assumption

$$\frac{\mathrm{d}\rho}{\mathrm{d}t} = \frac{\rho_0(z) - \rho}{V}\frac{\mathrm{d}V}{\mathrm{d}t} = \big(\rho_0(z) - \rho\big)\mu|\dot{\boldsymbol{x}}|. \tag{16}$$

Maxworthy's assertion that the overall impulse of the fluid, $\frac{\rho_{00}}{2}\iiint \boldsymbol{x}\times\boldsymbol{\omega}\,\mathrm{d}V$, is conserved is now extended to derive an equation of motion. The buoyancy force B is as in (10) giving a rate of change of vortex ring impulse

$$\frac{\mathrm{d}}{\mathrm{d}t}(\alpha\rho V\dot{\boldsymbol{x}}) = (\rho_0-\rho)Vg\hat{\boldsymbol{e}}_z, \tag{17}$$

where $\hat{\boldsymbol{e}}_z$ is a unit vector in the vertical direction and α is the coefficient (of order unity, analogous to Maxworthy's α) giving the impulse and dependent on the shape of the vortex. For instance $\alpha = 3/2$ for a Hill vortex and for definiteness this value is used throughout. With the inclusion of entrainment, (16), (17) leads to the nonlinear system of ordinary differential equations

$$\ddot{\boldsymbol{x}}(t) + \mu|\dot{\boldsymbol{x}}|\dot{\boldsymbol{x}} = \frac{\rho_0(z)-\rho}{\alpha\rho_{00}}g\hat{\boldsymbol{e}}_z, \tag{18}$$

$$\frac{\mathrm{d}\rho}{\mathrm{d}t} = \big(\rho_0(z)-\rho\big)\mu|\dot{\boldsymbol{x}}|. \tag{19}$$

The initial condition on the density is that $\rho(0)=\rho_{00}$ and the initial conditions on the position and velocity are $\boldsymbol{x}(0)=\boldsymbol{0}$ and $\dot{\boldsymbol{x}}(0)=\dot{\boldsymbol{x}}_0$. Note that the model given in (18), (19) contains the same unknown parameter (i.e. μ) as Maxworthy's model and that the inclusion of entrainment through a density stratification has not introduced any new parameters.

Since (18), (19) is a coupled nonlinear set of differential equations, an analytical solution was not attempted. Instead solutions were found numerically by time stepping solutions. Taking $\dot{\boldsymbol{x}} = (u, 0, w)$ it follows

$$\begin{cases} \dfrac{\mathrm{d}u}{\mathrm{d}t} = -\mu u\sqrt{u^2+w^2}, \\ \dfrac{\mathrm{d}w}{\mathrm{d}t} = -\mu w\sqrt{u^2+w^2} + \dfrac{\rho_0-\rho}{\alpha\rho_{00}}g, \\ \dfrac{\mathrm{d}\rho}{\mathrm{d}t} = \mu(\rho_0-\rho)\sqrt{u^2+w^2}. \end{cases} \tag{20}$$

The solution is iterated forward in time using the initial conditions.

The assumption that the fluid within the vortex ring is homogeneous is a strong simplifying assumption. One possible effect of this assumption is that the model forces the fluid being detrained behind the vortex ring to be of density ρ. However, if the fluid is not well mixed this may not be true and thus (15) may not be true.

3.3. Comparison with experiment

The vortex ring tracks shown in Fig. 11 are plotted again in Fig. 12 along with the theory given in Section 3.2. The dashed lines are the simplistic model, where the vortex ring remains at constant density, and the solid lines are the entraining model. The parameters $\dot{x}_0$ and μ are calculated from the first data points as in Section 2. Fig. 12 shows the tracks of the vortex rings. The data points are separated by time steps of 0.47 s. The dashed curve, always oscillates too high. This is due to neglecting the change in the density of the vortex ring. The solid curve shows the model predictions from (18), (19), with density entrainment allowed for. All experiments had initial downward motion for the vortex ring. This means that the solid curve always penetrates slightly further down into the fluid, and that all its subsequent maxima are lower than those of the dashed curve.

The entrainment model (solid) fits the data points much better than the simplistic model (dashed) where the vortex ring remains at constant density. Both models are poor approximations to the track of the vortex ring after the first complete oscillation. In the experiments shown, the vortex ring is then starting to collapse, thereby invalidating the model. The fits are much better for the higher Froude number experiments than for the low Froude number experiments. The vortex rings remain coherent for longer in the high Froude number experiments.

The density of the vortex ring changes because of the entrainment of the surrounding ambient fluid. The modelled ring density for the vortex ring in Fig. 12(f) is shown in Fig. 13. The vertical position of the vortex ring is shown as solid and the vortex ring density is shown as dot-dashed, both against time. The maximum density is indicated with a dotted line.

The time of maximum density of the vortex ring occurs after the time of minimum vertical position. As the vortex ring propagates downwards into denser fluid, the entrained fluid increases the vortex ring's density, changing its

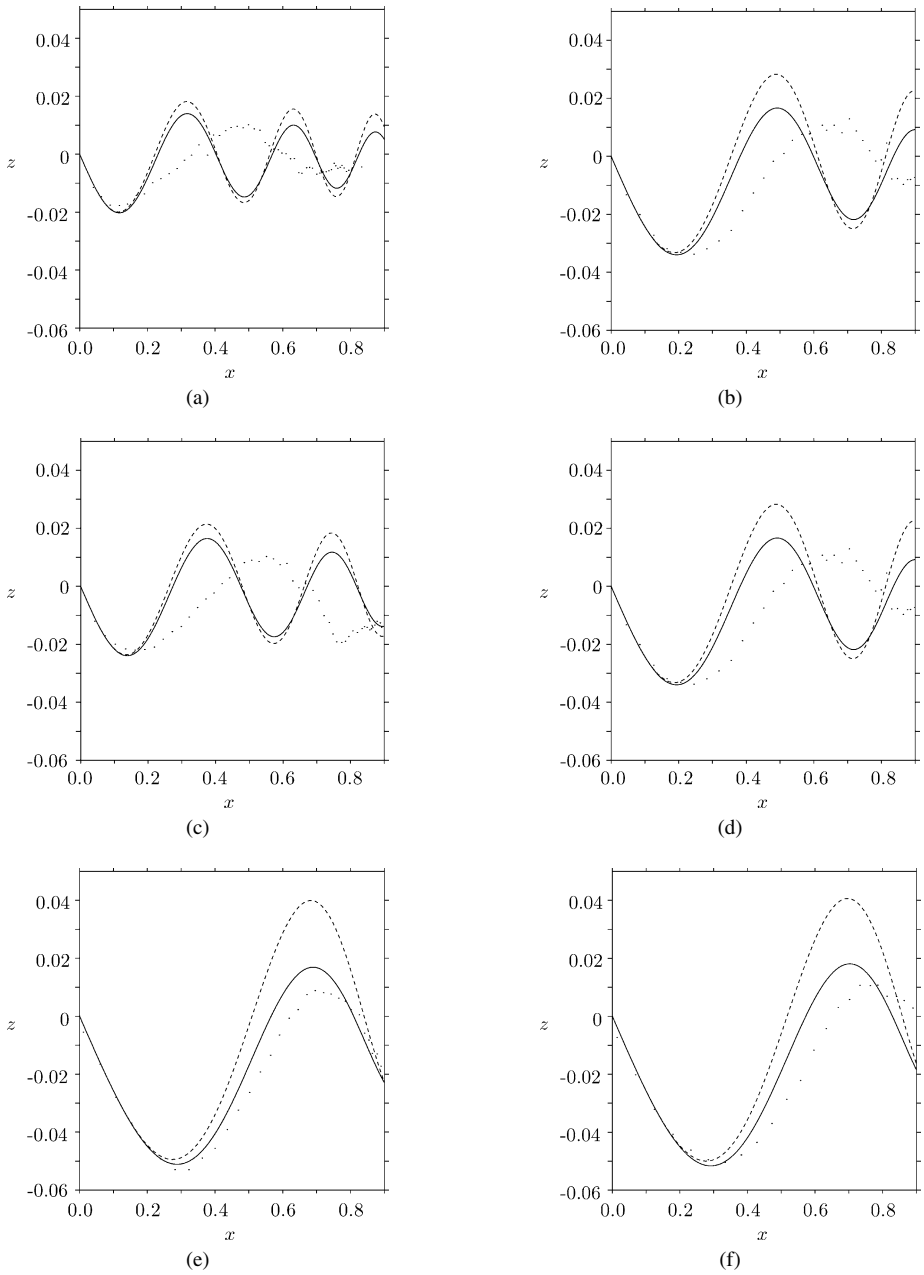

Fig. 12. Particle tracks; experimental (dots), simplistic model (dashed), entraining model (solid). Vortex rings fired at 105° to the vertical at; (a) $Fr = 2.2$, (b) $Fr = 2.5$, (c) $Fr = 3.0$, (d) $Fr = 4.1$, (e) $Fr = 5.3$ and (f) $Fr = 5.5$.

neutral buoyancy level. When the vertical direction of motion of the vortex ring changes at $t = 2.4$ s, the density of the vortex ring keeps increasing. The density of the vortex ring cannot start decreasing until it has risen above its instantaneous neutrally buoyant level. This happens at $t = 4.8$ s when the vortex ring is at its new neutrally buoyant height, $z = -0.013$ m (dashed line).

4. Conclusions

Turner's previous study (Turner [26,28]) of buoyancy forces on vortex rings was discussed in Section 3.1. Turner [26] showed that a very buoyant vortex ring rising through a stratified fluid entrains heavy fluid "in such a manner

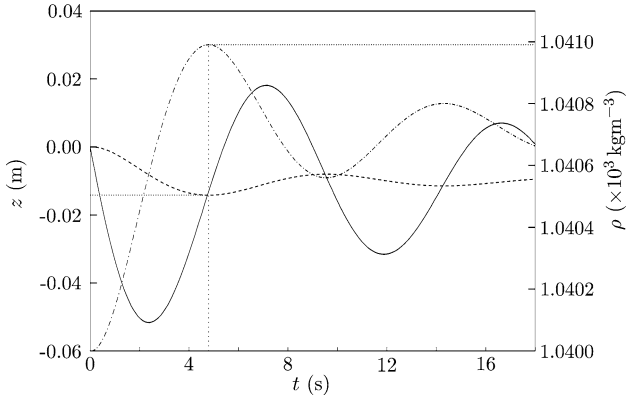

Fig. 13. The change in density of the vortex ring in Fig. 12(f) (dot-dashed) with the vertical position of the vortex ring (solid) against time. The dashed curve shows the instantaneous neutral density level of the vortex ring. Curves are calculated with the entrainment model (20). The dotted lines indicate that at $t = 4.8$ s, the vortex ring propagates above its neutral buoyancy level ($z = -0.013$ m) for the first time and hence the density of the vortex ring starts decreasing for the first time.

that heavy fluid is inside lighter layers". One might expect convective instability to result. Such an instability may cause the vortex ring to break down and thus to have a lower maximum rise height than a non-buoyant vortex ring. The problem Turner considers is different from the present one in two ways. Firstly the vortex rings are allowed to be buoyant initially, meaning that the impulse of the vortex ring is not conserved throughout the flow. Secondly, for a vertically propagating vortex ring, in particular a *buoyant* vertically propagating vortex ring, the density differences are such that it is not clear that the Boussinesq approximation (Boussinesq [22]) remains valid.

Section 3.2 reformulated and extended Maxworthy's [5] model for vortex ring propagation. It was seen that a vortex ring propagating through a homogeneous fluid could be considered to be a body translating, whilst experiencing a velocity-squared drag force. This model was then extended to include a simple restoring buoyancy force. It was shown (Fig. 12) that without allowing the vortex ring to entrain ambient background fluid of differing density to that of the vortex ring that the model over predicted the size of oscillation of the vortex ring's path. However, when entrainment was allowed, the model, at least initially, predicts the path of the vortex ring reasonably well (Section 3.3). It was seen that the best agreement was in the higher Froude number flows.

Since the best model predictions are from the high Froude number flows, it is suggested that a possible reason for the poor fit of the lower Froude number flows, even at early times before collapse, is due to internal wave generation. As the vortex ring propagates and internal waves are generated, the vortex ring may be expected to feel a wave resistance. The whole motion, vortex ring and waves, originates from the initial impulse given to the vortex ring. Hence, since impulse, given by

$$\boldsymbol{I} = \frac{\rho_{00}}{2} \iiint \boldsymbol{x} \times \boldsymbol{\omega} \, \mathrm{d}V, \tag{21}$$

is conserved, the deceleration of the vortex ring may be expected to be greater than in a homogeneous fluid. Further discussion of these effects may be found in Scase [31].

Acknowledgements

The authors wish to thank the technicians of the G. K. Batchelor laboratory in DAMTP, in particular Mr. D. Page-Croft and Mr. B. Dean for the manufacture of the experimental equipment. This work was funded by the Natural Environment Research Council under grant NER/S/A/2000/03262.

References

[1] P. Holmes, J.L. Lumley, G. Berkooz, Turbulence, Coherent Structures, Dynamical Systems and Symmetry, Cambridge University Press, 1996.
[2] K. Bryan, M.D. Cox, An approximate equation of state for numerical models of ocean circulation, J. Phys. Oceanogr. 2 (1972) 510–514.
[3] A.E. Gill, Atmosphere–Ocean Dynamics, Academic Press, 1982.

[4] M.J. Lighthill, Waves in Fluids, Cambridge University Press, 1978.
[5] T. Maxworthy, The structure and stability of vortex rings, J. Fluid Mech. 51 (1972) 15–32.
[6] P.F. Linden, The interaction of a vortex ring with a sharp density interface: a model for turbulent entrainment, J. Fluid Mech. 60 (1973) 467–480.
[7] J.S. Turner, The influence of molecular diffusivity on turbulent entrainment across a density interface, J. Fluid Mech. 33 (1968) 639–656.
[8] L.E. Fraenkel, On steady vortex rings of small cross-section in an ideal fluid, Proc. Roy. Soc. London Ser. A 316 (1970) 29–62.
[9] L.E. Fraenkel, Examples of steady vortex rings of small cross-section in an ideal fluid, J. Fluid Mech. 51 (1972) 119–135.
[10] J. Norbury, A family of steady vortex rings, J. Fluid Mech. 57 (1973) 417–431.
[11] M.J.M. Hill, On a spherical vortex, Philos. Trans. Roy. Soc. London Ser. A (185) (1894) 213–245.
[12] O. Reynolds, On the resistance encountered by vortex rings, and the relation between the vortex ring and the streamlines of a disk, Nature 14 (1876) 477.
[13] S.E. Widnall, J.P. Sullivan, On the stability of vortex rings, Proc. Roy. Soc. London Ser. A 332 (1973) 335–353.
[14] S.E. Widnall, C.-Y. Tsai, The instability of the thin vortex ring of constant vorticity, Philos. Trans. Roy. Soc. London Ser. A 287 (1977) 273–305.
[15] R. Fjørtoft, On the changes in the spectral distribution of kinetic energy for two-dimensional, nondivergent flow, Tellus 5 (1953) 225–230.
[16] J.G. Charney, Geostrophic turbulence, J. Atmospheric Sci. 28 (1971) 1087–1095.
[17] B. Fornberg, A numerical study of 2-D turbulence, J. Comput. Phys. 25 (1977) 1–31.
[18] J.C. McWilliams, The emergence of isolated coherent vortices in turbulent flow, J. Fluid Mech. 146 (1984) 21–43.
[19] G.J.F. van Heijst, Self-organisation of two-dimensional flows, http://www.fluid.tue.nl/WDY/vort/ntvn/selforg.html, Eindhoven University of Technology, 1993. An adapted version of a Dutch publication that appeared in Nederlands Tijdschrift voor Natuurkunde 59 (1993) 321–325.
[20] J.B. Flór, G.J.F. van Heijst, An experimental study of dipolar vortex structures in a stratified fluid, J. Fluid Mech. 279 (1994) 101–133.
[21] P. Orlandi, P. Egermann, E.J. Hopfinger, Vortex rings descending in a stratified fluid, Phys. Fluids 10 (11) (1998) 2819–2827.
[22] J. Boussinesq, Théorie analytique de la chaleur, vol. 2, Gathier-Villars, Paris, 1903.
[23] N. Didden, Untersuchung laminarer instabiler ringwirbel mittels laser-Doppler-anemomemtrie, No. 64, 1977.
[24] M. Van Dyke, An Album of Fluid Motion, Parabolic Press, Stanford, CA, 1982.
[25] J.M.H. Fortuin, Theory and application of two supplementary methods of constructing density gradient columns, J. Polym. Sci. 44 (1960) 505–515.
[26] J.S. Turner, Buoyant vortex rings, Proc. Roy. Soc. London Ser. A (239) (1957) 61–75.
[27] J.S. Turner, The flow into an expanding spherical vortex, J. Fluid Mech. 18 (1964) 195–208.
[28] J.S. Turner, Buoyancy Effects in Fluids, Cambridge University Press, 1995.
[29] H. Lamb, Hydrodynamics, sixth ed., Cambridge University Press, 1932.
[30] G.K. Batchelor, An Introduction to Fluid Dynamics, Cambridge Mathematical Library, Cambridge University Press, 1967, 2000 edition.
[31] M.M. Scase, Vortex rings in a stratified fluid, Ph.D. Thesis, University of Cambridge, 2003.